servations can be rationalized, to some degree, by examining the molecular orbitals available for metal–metal bonding in these bioctahedral systems.[14] There are six d orbitals available for M–M bonding originaing from the two t_{2g} sets of each ruthenium atom. From symmetry considerations they are able to form σ, σ^*, π, π^*, δ, and δ^* combinations whose relative energies are given in Figure 5. The reversal in the ordering of the δ and δ^* levels has its origin in a δ-orbital symmetry match with the bridging oxygen ligands.[14a] The electronic configuration for $[L_{OEt}(H_2O)Ru(\mu\text{-}O)_2Ru(OH_2)L_{OEt}][CF_3SO_3]_2$ and $[L_{OEt}(HO)Ru(\mu\text{-}O)_2Ru(OH)L_{OEt}]$ is d^4–d^4 and therefore implies a double bond ($\sigma^2\pi^2\delta^{*2}\delta^2$), which is consistent with the measured Ru–Ru distances. The d^3–d^3 configuration of $[L_{OEt}(O)Ru(\mu\text{-}O)_2Ru(O)L_{OEt}]$, because of the δ/δ^* reversal, would be expected to exhibit a slightly weaker metal–metal interaction. (Obviously, this reversal is not manifest in the d^4–d^4 case.) However, because the δ orbital is only weakly bonding and the δ^* orbital only weakly antibonding, the reversal alone is not expected to account for the very large increase observed in the Ru–Ru distance. A second and possibly a more compelling factor is the increase in effective nuclear charge ($Ru^{IV} \rightarrow Ru^{V}$), which would lead to less diffuse metal orbitals and hence to a weaker metal–metal interaction (represented as a contraction of the energy levels in Figure 5). This latter factor is presumably the major contributor to the lengthening of the Ru–Ru distance.

Finally, in light of long Ru–Ru separation and presumably weak interaction, it is significant that $[L_{OEt}(O)Ru(\mu\text{-}O)_2Ru(O)L_{OEt}]$ appears to be diamagnetic at room temperature, which must imply some strong coupling of the d^3–d^3 system. Whether this coupling occurs via the weak metal–metal interaction or by some other mechanism, such as superexchange mediated by the bridging oxo ligands, is unknown.[15]

(14) (a) Shaik, S.; Hoffmann, R.; Fisel, C. R.; Summerville, R. H. *J. Am. Chem. Soc.* **1980**, *102*, 4555. (b) Cotton, F. A. *Polyhedron* **1987**, *6*, 667.

Conclusions

The edge-sharing bioctahedral ruthenium complexes $[L_{OEt}(H_2O)Ru(\mu\text{-}O)_2Ru(OH_2)L_{OEt}][CF_3SO_3]_2$, $[L_{OEt}(HO)Ru(\mu\text{-}O)_2Ru(OH)L_{OEt}]$, and $[L_{OEt}(O)Ru(\mu\text{-}O)_2Ru(O)L_{OEt}$ have been synthesized under relatively strong oxidizing conditions. These results, particularly the synthesis of the Ru^V–Ru^V oxo system, clearly indicate the oxidative robustness and the viability of the L_{OEt}^- ligand in high-oxidation-state ruthenium oxo chemistry. The structural studies have revealed a considerable metal-metal interaction in the Ru^{IV}–Ru^{IV} systems, while the Ru^V–Ru^V complex is unexpectedly found to be diamagnetic despite a scant metal–metal interaction. The reactivity of these complexes, particularly the Ru^V–Ru^V oxo complex, will be the topic of future reports.

Acknowledgment. This work was supported by the Caltech Consortium in Chemistry and Chemical Engineering (founding members E. I. du Pont de Nemours and Co., Inc., Eastman Kodak Co., Minnesota Mining and Manufacturing Co., and Shell Development Co.). K.E. thanks the Deutsche Forschungsgemeinschaft (Germany) for a stipend. We thank Professor Philip P. Power and Mr. Steven C. Shoner for the crystal structure of $[L_{OEt}(HO)Ru(\mu\text{-}O)_2Ru(OH)L_{OEt}]$.

Supplementary Material Available: Crystal and intensity collection data (Tables S1–S3); complete distances and angles (Tables S4–S6), and anisotropic thermal displacement parameters (Tables S7–S9) for $[L_{OEt}(H_2O)Ru(\mu\text{-}O)_2Ru(OH_2)L_{OEt}][CF_3SO_3]_2$, $[L_{OEt}(HO)Ru(\mu\text{-}O)_2Ru(OH)L_{OEt}]$, and $[L_{OEt}(O)Ru(\mu\text{-}O)_2Ru(O)L_{OEt}]$ and assigned hydrogen parameters (Tables S10 and S11) for $[L_{OEt}(H_2O)Ru(\mu\text{-}O)_2Ru(OH_2)L_{OEt}][CF_3SO_3]_2$ and $[L_{OEt}(O)Ru(\mu\text{-}O)_2Ru(O)L_{OEt}]$ only (18 pages); observed and calculated structure factors (Tables S12–S14) for all three complexes (67 pages). Ordering information is given on any current masthead page.

(15) Weaver, T. T.; Meyer, T. J.; Adeyemi, S. A.; Brown, G. M.; Eckbert, R. P.; Hatfield, W. E.; Johnson, E. C.; Murray, R. W.; Untereker, D. *J. Am. Chem. Soc.* **1975**, *97*, 3039. Armstrong, J. W.; Robinson, W. R.; Walton, R. A. *Inorg. Chem.* **1983**, *22*, 1301. Neubold, P.; Wieghardt, K.; Nuber, B.; Weiss, J. *Inorg. Chem.* **1989**, *28*, 459.

Contribution from the Departments of Chemistry, Washington University, St. Louis, Missouri 63130, and Louisiana State University, Baton Rouge, Louisiana 70803-1804

Conformational Studies on Nickel, Palladium, and Platinum Homobimetallic Complexes Based on a Binucleating Hexaphosphine Ligand System

Suzanne E. Saum,[1a] Scott A. Laneman,[1b] and George G. Stanley*[,1b]

Received January 24, 1990

The reaction of 2 equiv of $NiCl_2 \cdot 6H_2O$, Na_2PdCl_4, or K_2PtCl_4 with the hexaphosphine ligand system $(Et_2PCH_2CH_2)_2PCH_2P(CH_2CH_2PEt_2)_2$, eHTP, produces the diamagnetic homobimetallic species, $M_2Cl_2(eHTP)^{2+}$ (M = Ni, **2**; Pd, **3**; Pt, **4**) in good yields. Single-crystal X-ray structures were performed on the PF_6^- salts of all three systems: Ni, monoclinic $C2/c$, a = 21.901 (7) Å, b = 18.639 (6) Å, c = 21.964 (6) Å, β = 95.42 (4)°, V = 8926 (7) Å^3, Z = 8; Pd, orthorhombic $P2_12_12_1$, a = 14.646 (1) Å, b = 16.761 (4) Å, c = 17.882 (2) Å, V = 4390 (2) Å^3, Z = 4; Pt, orthorhombic $P2_12_12_1$, a = 13.418 (3) Å, b = 17.795 (6) Å, c = 18.906 (4) Å, V = 4514 (4) Å^3, Z = 4. The final discrepancy indices (R values) are 0.092, 0.039, and 0.035 with quality of fit indicators of 3.25, 1.20, and 1.00 for the Ni, Pd, and Pt structures, respectively. The structure on the nickel bimetallic system reveals a distorted square-planar environment about the nickel atoms with the eHTP ligand adopting a symmetrical bis chelating/bridging open-mode coordination geometry with a Ni–Ni separation of 5.885 (1) Å. The Pd and Pt structures are isomorphous and similar to the Ni complex in the sense that the metal centers have distorted square-planar coordination geometries with one chloride and three phosphine ligands but differ quite substantially from the nickel system in that they have eHTP conformations with partially closed-mode structures and M–M separations of 4.4217 (8) and 4.6707 (9) Å, respectively. van der Waals energy calculations were performed on model systems using the SYBYL molecular mechanics/graphics program. The results demonstrate that there are a variety of accessible low-energy rotational conformations for these M_2(eHTP) bimetallic systems.

Introduction

The hextertiary phosphine $(Et_2PCH_2CH_2)_2PCH_2P(CH_2CH_2PEt_2)_2$, eHTP, possesses an unusual combination of bridging and chelating ligand functionalities: a central bis(phosphino)methane unit fused together with two tridentate, bis chelating moieties. eHTP was designed to act as a powerful binucleating ligand for transition-metal centers, and so far in every reaction in which 2 equiv of a simple mononuclear metal halide has been added to 1 equiv of eHTP a bimetallic complex has been observed.[2,3] An interesting aspect of the coordination chemistry

(1) (a) Washington University. (b) LSU.

(2) Askham, F. R.; Stanley, G. G.; Marques, E. C. *J. Am. Chem. Soc.* **1985**, *107*, 7423.

(3) Saum, S. E.; Askham, F. R.; Fronczek, F. R.; Stanley, G. G. *Organometallics* **1988**, *7*, 1409.

0020-1669/90/1329-5065$02.50/0

of eHTP, however, is that the closed-mode geometry **1a** has been the exception rather than the rule in the systems we have characterized. Bimetallic M_2(eHTP) systems have a remarkable propensity for rotations about the central methylene bridge to give open-mode binuclear systems such as **1b** and **1c** in which the metal centers are typically separated by 4–7 Å.

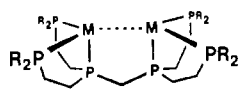

1a

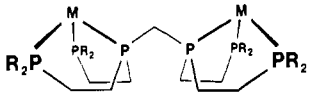

1b

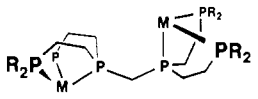

1c

The original reason for studying bimetallic eHTP complexes of the nickel triad was to see if eHTP could adopt a square-planar coordination geometry with two fused transoidal five-membered phosphorus chelate rings. This was prompted by the structural characterization of *mer,mer*-Cr_2Cl_6(eHTP), which has the eHTP conformation shown below.[4] The chromium(III) atoms are in a distorted octahedral environment with a meridional set of three chloride and phosphine ligands. In order to attain this mer geometry, the eHTP ligand adopts a coordination mode in which the phosphine atoms P2–P1–P3, instead of acting as an independent bis chelating group to one Cr atom, span the two chromium centers to give a P1–P2 chelate to one metal atom while P3 bridges to the other Cr center. This gives rise to fused five- and seven-membered ring systems for the Cr_2(eHTP) moiety. It turns out that the eHTP ligand adopts this geometry mainly because of the long Cr–P bonds (ca. 2.5 Å) that are present and the strong electronic preference for $CrCl_3P_3$ systems to have a meridional arrangement of ligands.[4] If the eHTP ligand coordinated to the Cr atom by using P3–P1–P2, the presence of two fused transoidal five-membered eHTP chelate rings and the long Cr–P bonds would produce considerably more steric strain than that seen for the multibridging configuration found in *mer,mer*-Cr_2Cl_6(eHTP).

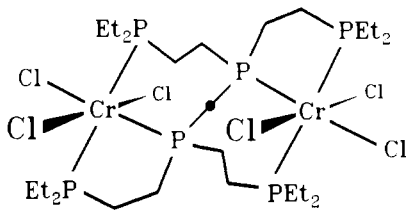

The M_2Cl_2(eHTP)$^{2+}$ (M = Ni, Pd, Pt) series of complexes clearly demonstrate that eHTP can indeed coordinate to a square-planar metal center in a more traditional fashion. Since the HTP ligand framework was *not* designed to allow closed-mode geometries when the terminal phosphorus groups are in a transoidal orientation, it was hardly surprising that structures on the Cl^- and BF_4^- salts of Ni_2Cl_2(eHTP)$^{2+}$ revealed open-mode geometries with Ni–Ni separations of 5.7 to 5.9 Å.[5]

In marked contrast to the open-mode rotational conformers seen for the nickel compounds, the structure of the PF_6^- salt of Pt_2Cl_2(eHTP)$^{2+}$ was observed to have a partially closed mode eHTP configuration with a Pt–Pt separation of 4.6707 (9) Å.[6] In order to study the differences between these systems in more detail, we would now like to report a full conformational study on homobimetallic eHTP complexes of the nickel triad. Crystal structures on the PF_6^- salts of M_2Cl_2(eHTP)$^{2+}$ (M = Ni, Pd, Pt) along with van der Waals energy calculations on the Ni and Pd compounds are presented and discussed.

Experimental Section

Unless stated otherwise all procedures were carried out under inert atmosphere (prepurified nitrogen or argon) by using standard Schlenk line or glovebox techniques. eHTP was prepared according to published procedures.[2] IR spectra were run on a Perkin-Elmer 283B spectrometer; UV–vis spectra were run on a Cary 218 spectrophotometer; NMR spectra were obtained on the following Bruker Fourier transform spectrometers: AC-100, AC-200, and AM-400. ^{1}H NMR spectra were referenced to solvent peaks (relative to TMS) while ^{31}P NMR spectra were referenced to H_3PO_4. Elemental analyses were performed by Oneida Research Services, Inc., Whitesboro, NY.

[Ni_2Cl_2(eHTP)](PF_6)$_2$ (2). eHTP (1.018 g, 1.87 mmol) in 20 mL of EtOH was added dropwise to 0.888 g (3.74 mmol) of $NiCl_2 \cdot 6H_2O$ in 20 mL of EtOH. The solution rapidly turns from green to dark brown-red. After the addition is complete, the solution is stirred for 5 min and evaporated to dryness to form crude [Ni_2Cl_2(eHTP)]$(Cl)_2$ in quantitative yield. The PF_6^- salt is obtained as a yellow-orange precipitate from the addition of 2 equiv of $AgPF_6$ to a concentrated methanol solution of the chloride salt. The solid is collected by filtration and dissolved in methanol. Slow evaporation of this solution yielded X-ray quality crystals. The crude product can also be recrystallized by slow evaporation of a 70/20/10 mixture of CH_2Cl_2/toluene/hexane and washed with 3–5 mL of cold CH_2Cl_2 to give orange-red crystals in a yield of 60%. **2** is an air-stable solid, although solutions slowly react over the course of a week or two with oxygen to give unidentified green solutions. **2** is soluble in polar organic solvents and the chloride salt is also soluble in water.

Anal. Calcd for $C_{25}H_{58}Cl_2P_8F_{12}Ni_2$: C, 29.34; H, 5.58. Found: 29.14; H, 5.59. ^{31}P NMR on **2** (CH_2Cl_2, ppm): 103.8 (pseudoquintet, 2 P, J_{P-P} = 30 Hz) 56.2 (pseudodoublet, 4 P, J_{P-P} = 44 Hz). ^{1}H NMR on PF_6^- salt (acetone-d_6, ppm): 1.28 (t, PCH_2CH_3, J_{P-H} = 18.0 Hz, J_{H-H} = 7.8 Hz), 1.32 (t, PCH_2CH_3, J_{P-H} = 18.0 Hz, J_{H-H} = 7.8 Hz), 2.13 (q, PCH_2CH_3, J_{P-H} = 10.2 Hz, J_{H-H} = 7.8 Hz), 2.18 (q, PCH_2CH_3, J_{P-H} = 11.7 Hz, J_{H-H} = 7.8 Hz), 2.15 (ddd, PCH_2CH_2P, J_{P-H} = 10.3 Hz, J_{H-H} = 15.4 Hz, J_{H-H} = 7.8 Hz, J_{H-H} = 3.9 Hz), 2.23 (ddd, PCH_2CH_2P, J_{P-H} = 9.7 Hz, J_{H-H} = 15.4 Hz, J_{H-H} = 7.8 Hz, J_{H-H} = 2.7 Hz), 2.92 (ddd, PCH_2CH_2P, J_{P-H} = 13.6 Hz, J_{H-H} = 15.7 Hz, J_{H-H} = 7.2 Hz, J_{H-H} = 2.3 Hz), 3.03 (dd, PCH_2CH_2P, J_{P-H} = 13.6 Hz, J_{H-H} = 14.0 Hz, J_{H-H} = 7.2 Hz), 3.35 (t, P–CH_2–P, J_{P-H} = 11.2 Hz). UV–vis spectral data (CH_2Cl_2): Cl^- salt, 406 nm (ϵ = 3984), 272 nm (ϵ = 37280), 226 nm (ϵ = 33590); PF_6^- salt, 406 nm (ϵ = 3555), 272 nm (ϵ = 29380), 224 nm (ϵ = 28970).

[Pd_2Cl_2(eHTP)](PF_6)$_2$ (3). Method A. $PdCl_2$ (0.200 g, 1.13 mmol) and NaCl (0.132 g, 2.25 mmol) were stirred and heated in 20 mL of water until all the $PdCl_2$ dissolved. The resulting Na_2PdCl_4 solution was added slowly to eHTP (0.307 g, 0.56 mmol) in 20 mL of ethanol. The solution immediately turned orange and the reaction mixture was allowed to stir overnight. The solvent was evaporated to dryness leaving an orange solid representing crude Pd_2Cl_2(eHTP)$^{2+}$ in about 70% yield. The PF_6^- salt was prepared by dissolving the orange solid in methanol followed by the addition of excess $NaPF_6$. The white precipitate was collected by filtration, washed with cold methanol (50% isolated yield) and recrystallized by very slow evaporation from acetone to yield a few colorless X-ray quality crystals.

Method B. The Cl^- salt of Pd_2Cl_2(eHTP)$^{2+}$ can also be prepared by using $PdCl_2$(benzonitrile)$_2$ as the starting material.[7] $PdCl_2$(benzonitrile)$_2$ (0.500 g, 1.3 mmol) was dissolved in 20 mL of THF and slowly added to a stirred solution of eHTP (0.355 g, 0.65 mmol) in 20 mL of THF. The solution immediately turned orange and the product was isolated as in method A with similar yields. IR (KBr, cm^{-1}): 2960, 2935, 2900, 2880 (m, C–H); 1455, 1415 (m, C–C); 1045, 1030 (m, P–Et). ^{31}P{^{1}H} NMR (acetone-d_6, ppm): 103.9 (s, 2 P), 56.2 (s, 1 P). There was a persistent minor impurity in the samples that had five broad ^{31}P signals at 30.4, 33.7, 58.1, 76.4, and 79.7 ppm. Because of this impurity and the fact that only a few single crystals were obtained, an elemental analysis was not performed on this compound.

[Pt_2Cl_2(eHTP)](PF_6)$_2$ (4). K_2PtCl_4 (0.428 g, 1.03 mmol) was dissolved in 15 mL of water and added dropwise to eHTP (0.280 g, 0.515 mmol) in 15 mL of ethanol. The solution, which immediately turned yellow, was stirred for 24 h. The solvents were removed by vacuum evaporation and the resulting yellow solid was washed with several 2-mL portions of acetonitrile to yield crude white [Pt_2Cl_2(eHTP)]$(Cl)_2$ in 90% yield. The PF_6^- salt was prepared by dissolving 0.300 g (0.28 mmol) of [Pt_2Cl_2(eHTP)]$(Cl)_2$ in water to which an aqueous solution containing

(4) Askham, F. R.; Maverick, A. W.; Stanley, G. G. *Inorg. Chem.* **1987**, *26*, 3963.
(5) Laneman, S. A.; Stanley, G. G. *Inorg. Chem.* **1987**, *26*, 1177.
(6) Saum, S. E.; Stanley, G. G. *Polyhedron* **1987**, *6*, 1803.
(7) Doyle, J. R.; Slade, P. E.; Jonassen, H. B. *Inorg. Synth.* **1960**, *6*, 218.

Table I. Crystallographic Data for $M_2Cl_2(eHTP)^{2+}$ (M = Ni, Pd, Pt)

formula	$Ni_2Cl_2P_8F_{12}C_{25}H_{58}$	$Pd_2Cl_3P_7F_6O_3C_{25}H_{64}$	$Pt_2Cl_2P_8F_{12}C_{25}H_{58}$
fw	1022.84	1062.75	1293.58
space group	$C2/c$ (No. 15)	$P2_12_12_1$ (No. 19)	$P2_12_12_1$ (No. 19)
a, Å	21.901 (7)	14.646 (1)	13.418 (3)
b, Å	18.639 (6)	16.761 (4)	17.795 (6)
c, Å	21.964 (6)	17.882 (2)	18.906 (4)
β, deg	95.42 (4)	90.00	90.00
V, Å^3	8926 (7)	4390 (2)	4514 (4)
Z	8	4	4
d_{calc}, g/mL	1.52	1.59	1.90
μ(Mo Kα), cm^{-1}	13.19	12.9	67.23
temp, °C	23	23	25
radiation	Mo Kα, 0.71073 Å	Mo Kα	Mo Kα
$R(F_o)$	0.092	0.039	0.035
$R_2(F_o)$	0.128	0.052	0.047
range of transm coeff		0.9062–0.9991	0.8145–0.9989

excess $NaPF_6$ was added causing a white precipitate to form. The solid was collected by filtration and recrystallized from acetone/ethanol/water to produce X-ray quality single crystals. As with the nickel and palladium complexes, the platinum system is soluble in polar organic solvents such as THF, CH_2Cl_2, EtOH, and MeOH. The parent chloride salt is also soluble in water.

Anal. Calcd for $C_{25}H_{58}P_8Cl_2F_{12}Pt_2$: C, 23.18; H, 4.51; P, 19.12. Found: C, 23.48; H, 4.53; P, 18.93. IR (KBr, cm^{-1}): 2970, 2940, 2880 (m, C–H); 1460, 1440, 1385 (m, C–C); 1050, 1030 (m, P–Et), 550 (s, P–F). $^{31}P\{^1H\}$ NMR (acetone-d_6, ppm): 51.3 (s, 2 P, J_{Pt-P} = 1144.5 Hz), 79.3 (s, 1 P, J_{Pt-P} = 1572 Hz).

X-ray Crystallography. Crystals were mounted at the end of glass fibers with epoxy. Data sets on the Ni and Pt structures were collected with a Nicolet P3 diffractometer, while the Pd structure was done on a Enraf-Nonius CAD4 system. All structures made use of Mo Kα radiation and the $\theta/2\theta$ scan data collection technique. Three standard reflections measured every 100 data points showed no significant change in intensity. Data were corrected for Lorentz and polarization effects but were not corrected for extinction. Empirical absorption corrections were done either by the program DIFABS (Pt structure) or based on ψ scans of reflections near χ = 90° (Pd structure). The structures were solved by use of the Enraf-Nonius Structure Determination Package via the MULTAN direct methods programs on a microVAX II computing system. Table I lists information about the data collection and solution, while Tables II–V list the positional parameters and selected bond distances and angles for all three structures. Tables of anisotropic thermal parameters, and calculated and observed structure factors are provided in supplementary material.

The nickel structure was not particularly good based on the rather high discrepancy indices and GOF. This is mainly due to the poorly diffracting nature of the crystals obtained from the PF_6^- salt. Two independent crystals were used and similar low-quality data sets were collected on both Nicolet and Enraf-Nonius diffractometers. Part of the problem also may arise from the fact that there is disordering of some the ethyl groups on the eHTP ligand and the PF_6^- counterion. Refinement of the structure under the alternate space group Cc gave considerably poorer discrepancy indices and structural parameters.

The palladium structure turned out to be on a crystal of the mixed Cl^-/PF_6^- salt. We subsequently discovered that an excess of $NaPF_6$ must be used to get complete exchange of the initial chloride salt of $Pd_2Cl_2(eHTP)^{2+}$. The Cl^- and PF_6^- positions were not mixed between each other and Cl^- was identified as such by the lack of any residual electron density about its site. The PF_6^- group was disordered, but it was possible to model the disorder with three sets of six interleaved fluoride ligands. Further evidence for the presence of a mixed Cl^-/PF_6^- salt of **3** was provided by the ^{31}P NMR spectra of this sample and the fully exchanged PF_6^- salt. The intensity of the ^{31}P PF_6^- signals in the fully exchanged sample was twice that of the mixed Cl^-/PF_6^- salt of **3**. There also were several water molecules present in the structure and their presence (although not the absolute number) was confirmed by ^1H NMR measurements.

The platinum structure had a rather severe disordering of one of the eHTP terminal ethyl groups that could not be modeled. This is the source of the unusually large thermal parameter on C34. Enantiomorphic refinements of the Pd and Pt structures were not attempted. The f'' factor for Pd is only 1.07, which is probably too small to differentiate between the two enantiomers, while the Pt structure had a R value that was low enough (0.035) to assume that the correct enantiomorph had been chosen.

van der Waals Energy Calculations. The van der Waals energy (VDW) calculations were done by the SYBYL molecular mechanics/graphics program package (version 5.1) on model systems of the PF_6^- salts of $Ni_2Cl_2(eHTP)^{2+}$ derived from the crystallographic coordinates with methyl groups replacing the ethyl groups on the terminal phosphorus atoms. Dummy atom types were used for the transition-metal atom

Table II. Positional Parameters for $[Ni_2Cl_2(eHTP)](PF_6)_2$

atom	x	y	z	B,[a] Å^2
Ni1	0.40040 (5)	0.85834 (6)	−0.12041 (5)	4.87 (3)
Ni2	0.22593 (6)	0.78042 (7)	−0.33031 (6)	5.96 (3)
C11	0.4970 (1)	0.8560 (2)	−0.1319 (2)	9.02 (9)
C12	0.1889 (2)	0.6984 (2)	−0.3937 (1)	8.86 (8)
P1	0.3041 (1)	0.8561 (1)	−0.1188 (1)	5.20 (6)
P2	0.4002 (2)	0.7506 (2)	−0.0799 (1)	7.32 (8)
P3	0.3938 (1)	0.9754 (2)	−0.1219 (1)	7.04 (7)
P4	0.2616 (1)	0.8571 (1)	−0.2650 (1)	5.26 (6)
P5	0.3209 (1)	0.7431 (2)	−0.3317 (1)	7.41 (7)
P6	0.1393 (2)	0.8412 (2)	−0.3347 (2)	8.01 (8)
P7	0.6853 (2)	0.0895 (2)	−0.1348 (2)	10.0 (1)
P8	0.5871 (2)	0.4401 (2)	−0.1030 (2)	8.6 (1)
F1	0.7562 (5)	0.0804 (6)	−0.1383 (5)	17.2 (4)
F2	0.6878 (7)	0.0073 (6)	−0.1201 (5)	18.8 (5)
F3	0.6211 (6)	0.0961 (8)	−0.1400 (8)	22.9 (5)
F4	0.6965 (5)	0.1678 (6)	−0.1526 (7)	19.0 (5)
F5	0.6755 (6)	0.0636 (6)	−0.2037 (4)	17.4 (4)
F6	0.7030 (6)	0.1108 (6)	−0.0698 (4)	16.7 (4)
F7	0.5442 (5)	0.4544 (8)	−0.1607 (5)	18.8 (4)
F8	0.5424 (5)	0.3954 (7)	−0.0748 (6)	21.9 (4)
F9	0.6301 (6)	0.4206 (8)	−0.0453 (6)	21.6 (5)
F10	0.6337 (5)	0.4899 (7)	−0.1296 (7)	24.8 (5)
F11	0.6273 (7)	0.3860 (6)	−0.1286 (6)	21.1 (5)
F12	0.5643 (8)	0.5109 (9)	−0.0855 (7)	26.9 (6)
C′	0.2571 (4)	0.8212 (5)	−0.1874 (4)	5.2 (2)
C11	0.2853 (5)	0.7913 (7)	−0.0612 (5)	8.1 (3)
C12	0.3219 (6)	0.7233 (7)	−0.0687 (6)	9.3 (4)
C13	0.2755 (5)	0.9452 (7)	−0.0999 (6)	9.1 (3)
C14	0.3135 (6)	1.0011 (7)	−0.1287 (7)	10.5 (4)
C21	0.4302 (9)	0.6768 (9)	−0.1296 (8)	13.9 (6)
C22	0.429 (1)	0.6021 (9)	−0.101 (1)	19.2 (9)
C23	0.4468 (9)	0.7497 (8)	−0.0074 (7)	15.8 (5)
C24	0.458 (1)	0.788 (1)	0.0303 (9)	18.4 (8)
C31	0.4237 (6)	1.0014 (8)	−0.0432 (6)	12.6 (4)
C32	0.4027 (8)	1.052 (1)	−0.0119 (8)	14.6 (6)
C33	0.4327 (8)	1.0333 (8)	−0.1778 (8)	17.0 (5)
C34	0.439 (2)	1.098 (2)	−0.178 (2)	15 (1)
C34′	0.487 (1)	1.051 (1)	−0.152 (2)	12.0 (9)
C41	0.3424 (5)	0.8736 (5)	−0.2738 (4)	6.0 (2)
C42	0.3721 (5)	0.8005 (6)	−0.2810 (5)	6.9 (3)
C43	0.2157 (6)	0.9418 (6)	−0.2697 (6)	8.5 (3)
C44	0.1478 (6)	0.9167 (7)	−0.2841 (6)	9.8 (4)
C51	0.3324 (8)	0.6463 (8)	−0.2971 (9)	14.4 (5)
C52	0.404 (1)	0.622 (1)	−0.290 (1)	19.4 (9)
C53	0.3488 (7)	0.747 (1)	−0.4080 (7)	16.3 (6)
C54	0.341 (1)	0.807 (2)	−0.4378 (8)	25 (1)
C61	0.0712 (6)	0.7912 (8)	−0.3112 (7)	9.7 (4)
C62	0.0878 (6)	0.759 (1)	−0.2491 (8)	12.0 (5)
C63	0.1089 (6)	0.8693 (9)	−0.4094 (7)	11.5 (5)
C64	0.161 (1)	0.914 (1)	−0.4430 (9)	17.5 (8)

[a] Anisotropically refined atoms are given in the form of the isotropic equivalent displacement parameter defined as: $(4/3)[a^2\beta(1,1) + b^2\beta(2,2) + c^2\beta(3,3) + ab(\cos\gamma)\beta(1,2) + ac(\cos\beta)\beta(1,3) + bc(\cos\alpha)\beta(2,3)]$.

Table III. Positional Parameters for $Pd_2Cl_2(eHTP)](Cl)(PF_6)\cdot 3H_2O$[a]

atom	x	y	z	B, Å²
Pd1	0.68265 (4)	0.35701 (3)	0.26319 (3)	2.536 (8)
Pd2	0.57855 (4)	0.53132 (3)	0.09834 (3)	2.620 (9)
Cl1	0.7637 (2)	0.4121 (1)	0.3640 (1)	4.52 (4)
Cl2	0.5100 (2)	0.6449 (1)	0.1513 (1)	4.86 (5)
Cl3	0.3786 (2)	0.2508 (2)	0.0085 (1)	4.57 (5)
P1	0.6065 (1)	0.2954 (1)	0.1730 (1)	2.61 (3)
P2	0.5420 (1)	0.4094 (1)	0.2982 (1)	3.08 (4)
P3	0.7970 (1)	0.2644 (1)	0.2395 (1)	3.23 (4)
P4	0.6391 (1)	0.4274 (1)	0.0412 (1)	2.57 (3)
P5	0.4550 (1)	0.5092 (1)	0.0200 (1)	2.86 (4)
P6	0.7275 (2)	0.5604 (1)	0.1352 (1)	3.46 (4)
P7	0.3245 (2)	0.5540 (2)	0.7518 (2)	5.97 (7)
F1	0.344 (1)	0.495 (1)	0.686 (1)	8.8 (4)*
F1′	0.404 (2)	0.590 (2)	0.685 (1)	6.5 (6)*
F1″	0.337 (2)	0.576 (2)	0.668 (2)	7.9 (7)*
F2	0.228 (1)	0.505 (1)	0.7668 (9)	8.9 (4)*
F2′	0.385 (2)	0.622 (2)	0.788 (2)	7.3 (7)*
F2″	0.421 (3)	0.570 (2)	0.786 (2)	9.9 (9)*
F3	0.2622 (9)	0.6069 (8)	0.6950 (7)	6.6 (3)*
F3′	0.382 (2)	0.465 (2)	0.751 (2)	8.8 (8)*
F4	0.410 (1)	0.594 (1)	0.7390 (9)	9.2 (4)*
F4′	0.300 (3)	0.470 (2)	0.707 (2)	10.0 (9)*
F4″	0.235 (2)	0.500 (2)	0.730 (1)	6.3 (5)*
F5	0.297 (1)	0.608 (1)	0.815 (1)	10.2 (5)*
F5′	0.280 (2)	0.549 (2)	0.828 (2)	8.5 (8)*
F5″	0.337 (2)	0.504 (2)	0.825 (2)	6.7 (6)*
F6	0.373 (1)	0.490 (1)	0.8001 (9)	8.3 (4)*
F6′	0.269 (2)	0.633 (2)	0.728 (2)	8.3 (7)*
O1	0.3098 (6)	0.7302 (5)	0.5872 (5)	7.4 (2)
O2	0.4465 (7)	0.6450 (7)	0.5091 (5)	9.0 (3)
O3	0.4812 (8)	0.4891 (7)	0.5706 (7)	10.5 (3)
C′	0.6178 (6)	0.3271 (4)	0.0745 (4)	3.1 (1)
C11	0.4861 (5)	0.2966 (5)	0.1956 (5)	3.3 (2)
C12	0.4600 (6)	0.3781 (6)	0.2260 (5)	4.3 (2)
C13	0.6479 (6)	0.1948 (4)	0.1698 (5)	3.4 (2)
C14	0.7526 (6)	0.1938 (5)	0.1718 (5)	3.5 (2)
C21	0.5108 (7)	0.3578 (6)	0.3844 (5)	4.7 (2)
C22	0.4156 (9)	0.376 (1)	0.4136 (7)	9.1 (4)
C23	0.5174 (7)	0.5139 (5)	0.3135 (5)	4.4 (2)
C24	0.5719 (8)	0.5502 (6)	0.3777 (6)	5.9 (2)
C31	0.9071 (6)	0.2998 (6)	0.2043 (6)	4.6 (2)
C32	0.9796 (6)	0.2348 (7)	0.1989 (7)	6.1 (3)
C33	0.8242 (7)	0.2136 (5)	0.3257 (5)	4.9 (2)
C34	0.7436 (9)	0.1890 (6)	0.3712 (7)	6.5 (3)
C41	0.5937 (6)	0.4267 (5)	−0.0533 (4)	3.2 (1)
C42	0.4900 (6)	0.4361 (5)	−0.0518 (4)	3.5 (2)
C43	0.7635 (6)	0.4396 (5)	0.0380 (5)	4.0 (2)
C44	0.7949 (6)	0.4771 (5)	0.1101 (6)	4.3 (2)
C51	0.4269 (6)	0.6009 (5)	−0.0276 (5)	3.6 (2)
C52	0.5088 (7)	0.6422 (6)	−0.0638 (6)	5.4 (2)
C53	0.3488 (5)	0.4707 (6)	0.0583 (5)	3.8 (2)
C54	0.2694 (6)	0.4642 (7)	0.0010 (6)	5.6 (2)
C61	0.7617 (8)	0.6416 (6)	0.0748 (6)	6.3 (2)
C62	0.853 (1)	0.672 (1)	0.0792 (9)	12.7 (6)
C63	0.7610 (8)	0.5889 (7)	0.2291 (5)	5.7 (2)
C64	0.726 (1)	0.662 (1)	0.2583 (9)	10.6 (5)

[a] Values with an asterisk were refined isotropically. The primed and double primed atoms represent the disordered fluoride atoms on the PF_6^- group. Anisotropically refined atoms are given in the form of the isotropic equivalent displacement parameter defined as: $(4/3)[a^2\beta(1,1) + b^2\beta(2,2) + c^2\beta(3,3) + ab(\cos\gamma)\beta(1,2) + ac(\cos\beta)\beta(1,3) + bc(\cos\alpha)\beta(2,3)]$.

centers and the VDW screening factors were set at half their default values. The only geometric parameters varied were rotations (5° increments) about the two P–CH_2–P bonds. No electrostatic factors were included in the energy calculations. The least-squares superposition of the model $Pd_2Cl_2(HTP)^{2+}$ molecule and modified nickel system with a 126.6° P–CH_2–P angle and the same rotational conformation as the palladium structure was accomplished by using the FIT function from SYBYL and designating P1, C′, and P4 on both molecules as the matching atoms on which to do the least-squares superposition.

Results

Structure of $[Ni_2Cl_2(eHTP)](PF_6)_2$. The reaction of 2 equiv of $NiCl_2\cdot 6H_2O$ with eHTP produces the diamagnetic binuclear complex $Ni_2Cl_2(eHTP)^{2+}$ (**2**), which has been isolated in crystalline form as the PF_6^- (**2c**) salt. An ORTEP plot of the $Ni_2Cl_2(eHTP)^{2+}$ cation of **2c** is shown in Figure 1 with a listing of selected bond distances and angles given in Table V. The structure will be discussed further in the sections below.

Table IV. Positional Parameters for $[Pt_2Cl_2(eHTP)](PF_6)_2$

atom	x	y	z	B, Å²
Pt1	0.56302 (4)	0.05373 (3)	0.88022 (3)	2.85 (1)
Pt2	0.69701 (4)	−0.12676 (3)	0.72814 (3)	3.25 (1)
C11	0.4850 (4)	0.1543 (2)	0.8215 (3)	5.2 (1)
C12	0.7898 (4)	−0.0868 (3)	0.6298 (3)	6.5 (1)
P1	0.6324 (3)	−0.0389 (2)	0.9392 (2)	3.22 (8)
P2	0.4250 (3)	0.0305 (2)	0.9492 (2)	3.51 (8)
P3	0.7225 (3)	0.0844 (2)	0.8419 (2)	3.65 (8)
P4	0.6082 (3)	−0.1701 (2)	0.8171 (2)	2.95 (7)
P5	0.5494 (3)	−0.0773 (2)	0.6844 (2)	3.20 (8)
P6	0.8191 (4)	−0.2082 (3)	0.7686 (3)	4.9 (1)
C′	0.622 (1)	−0.1350 (8)	0.9073 (7)	4.0 (3)
C11	0.569 (1)	−0.0426 (8)	1.0247 (7)	4.2 (3)
C12	0.459 (1)	−0.0410 (9)	1.0158 (9)	4.7 (4)
C13	0.766 (1)	−0.0195 (8)	0.948 (1)	5.2 (4)
C14	0.803 (1)	0.011 (1)	0.878 (1)	5.6 (4)
C21	0.313 (1)	−0.003 (1)	0.9063 (8)	5.3 (4)
C22	0.218 (1)	−0.009 (1)	0.953 (1)	7.8 (6)
C23	0.390 (1)	0.118 (1)	0.998 (1)	5.1 (4)
C24	0.474 (2)	0.155 (1)	1.033 (1)	7.0 (5)
C31	0.753 (1)	0.094 (1)	0.752 (1)	5.9 (4)
C32	0.862 (1)	0.102 (1)	0.735 (1)	7.2 (5)
C33	0.770 (2)	0.170 (1)	0.886 (7)	7.4 (6)
C34	0.720 (2)	0.236 (1)	0.887 (3)	23 (2)
C41	0.477 (1)	−0.164 (1)	0.7925 (8)	4.4 (4)
C42	0.457 (1)	−0.087 (1)	0.7542 (8)	5.1 (4)
C43	0.641 (1)	−0.2705 (8)	0.8287 (8)	4.3 (4)
C44	0.756 (1)	−0.276 (1)	0.830 (1)	5.1 (4)
C51	0.500 (1)	−0.1400 (9)	0.6134 (9)	4.3 (3)
C52	0.557 (2)	−0.137 (1)	0.5469 (9)	8.4 (6)
C53	0.541 (1)	0.0178 (8)	0.6518 (9)	4.5 (4)
C54	0.446 (2)	0.0394 (9)	0.621 (1)	7.3 (5)
C61	0.881 (2)	−0.263 (1)	0.698 (1)	7.3 (5)
C62	0.805 (2)	−0.296 (1)	0.648 (1)	8.0 (6)
C63	0.922 (1)	−0.164 (1)	0.817 (1)	6.3 (5)
C64	1.001 (2)	−0.222 (2)	0.833 (2)	12 (1)
P7	0.3190 (5)	−0.2757 (3)	0.9389 (3)	5.8 (1)
P8	0.6491 (4)	0.5140 (4)	0.2799 (3)	6.1 (1)
F1	0.265 (1)	−0.3507 (9)	0.9242 (9)	11.2 (5)*
F2	0.403 (1)	−0.305 (1)	0.888 (1)	12.2 (5)*
F3	0.354 (1)	−0.312 (1)	1.009 (1)	11.9 (5)*
F4	0.273 (2)	−0.231 (1)	0.872 (1)	13.6 (6)*
F5	0.379 (2)	−0.206 (1)	0.954 (1)	12.7 (5)*
F6	0.226 (2)	−0.251 (2)	0.982 (1)	16.7 (7)*
F7	0.604 (1)	0.4389 (8)	0.3154 (8)	9.8 (4)*
F8	0.558 (1)	0.5589 (9)	0.3064 (9)	11.8 (5)*
F9	0.744 (1)	0.4673 (7)	0.2552 (7)	8.5 (3)*
F10	0.693 (1)	0.5837 (9)	0.2405 (9)	11.4 (4)*
F11	0.703 (1)	0.5368 (8)	0.3499 (8)	10.5 (4)*
F12	0.594 (2)	0.496 (1)	0.209 (1)	13.3 (5)*

[a] Values with an asterisk were refined isotropically. Anisotropically refined atoms are given in the form of the isotropic equivalent displacement parameter defined as: $(4/3)[a^2\beta(1,1) + b^2\beta(2,2) + c^2\beta(3,3) + ab(\cos\gamma)\beta(1,2) + ac(\cos\beta)\beta(1,3) + bc(\cos\alpha)\beta(2,3)]$. The extremely large thermal parameter on C34 is due to a disordering of the C33–C34 ethyl group that could not be modeled. This disordering causes both an unusually large thermal parameter for C34 and short bond distance for C33–C34.

Structure of $[Pd_2Cl_2(eHTP)](PF_6)_2$. The reaction of 2 equiv of Na_2PdCl_4 with eHTP followed by methasis with excess $NaPF_6$ produces the bimetallic $[Pd_2Cl_2(eHTP)](PF_6)_2$ complex, **3**. The reaction of eHTP with palladium is not particularly clean typically giving only 50–70% yields and an unidentified orange side product. There is also a colorless, very persistent impurity that gives five broad peaks in the ^{31}P NMR spectrum, which has so far eluded isolation and identification.

An ORTEP plot of the $Pd_2Cl_2(eHTP)^{2+}$ cation portion of **3** is shown in Figure 3 with a listing of selected bond distances and angles given in Table V. The structure actually turned out to be on a crystal of the mixed Cl^-/PF_6^- salt. We subsequently dis-

Table V. Selected Bond Distances (Å) and Angles (deg) for $M_2Cl_2(eHTP)^{2+}$ (M = Ni, Pd, Pt)[a]

	Ni	Pd	Pt
M1–M2	5.885 (1)	4.4217 (8)	4.6707 (9)
M1–C11	2.156 (2)	2.348 (2)	2.352 (5)
M1–P1	2.114 (2)	2.216 (2)	2.197 (4)
M1–P2	2.197 (2)	2.326 (2)	2.302 (5)
M1–P3	2.187 (2)	2.322 (2)	2.325 (5)
M2–C12	2.173 (2)	2.352 (2)	2.348 (5)
M2–P4	2.122 (2)	2.206 (2)	2.200 (4)
M2–P5	2.196 (2)	2.319 (2)	2.320 (5)
M2–P6	2.203 (2)	2.331 (2)	2.317 (5)
P1–C′	1.860 (5)	1.848 (8)	1.82 (2)
C11–M1–P1	173.81 (8)	175.23 (8)	177.5 (2)
C11–M1–P2	93.93 (8)	95.34 (8)	92.6 (2)
C11–M1–P3	94.76 (8)	92.19 (8)	94.8 (2)
P1–M1–P2	86.25 (7)	85.74 (7)	85.3 (2)
P1–M1–P3	87.43 (7)	85.34 (7)	86.8 (2)
P2–M1–P3	156.28 (8)	160.11 (8)	163.6 (2)
C12–M2–P4	177.30 (8)	176.08 (8)	176.8 (2)
C12–M2–P5	93.69 (8)	92.28 (8)	93.2 (2)
C12–M2–P6	93.84 (8)	96.69 (9)	94.3 (2)
P4–M2–P5	86.24 (7)	84.69 (7)	86.7 (2)
P4–M2–P6	86.73 (7)	85.40 (8)	85.0 (2)
P5–M2–P6	167.11 (9)	159.24 (8)	163.5 (2)
M1–P1–C′	118.1 (2)	121.0 (2)	120.2 (6)
M2–P4–C′	109.4 (2)	120.8 (3)	122.7 (6)
P1–C′–P4	123.3 (3)	126.6 (4)	129.7 (9)

[a] Numbers in parentheses are estimated standard deviations in the least significant digit.

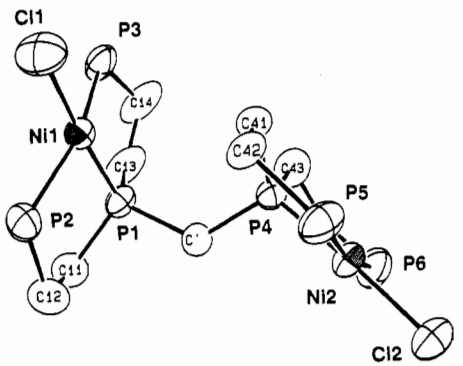

Figure 1. ORTEP plot of $[Ni_2Cl_2(eHTP)](PF_6)_2$, **2c**. Ethyl groups on the terminal phosphines have been omitted for clarity and the atom labeling scheme is the same as that used in previous eHTP structures. Thermal ellipsoids are shown at the 33% probability level.

covered that an excess of $NaPF_6$ must be used to give complete exchange of the initial chloride salt of $Pd_2Cl_2(eHTP)^{2+}$. The structure will be discussed further in the sections below.

van der Waals Energy Calculations on Ni and Pd Systems. The van der Waals (VDW) energy calculations in the nickel and palladium systems were performed with the SYBYL molecular graphics/mechanics programs.[8] We are limited to performing rather simple VDW energy calculations on a semistatic $M_2Cl_2(HTP)^{2+}$ molecule and not more sophisticated molecular mechanics methods because of the almost total lack of force fields for metal–ligand bonds. The development of accurate force fields for these systems is difficult because of the relatively weak nature of M–L and M–M bonding and the considerable influence of electronic effects on this bonding.

The atomic positions used in the VDW energy calculations were from the crystal structures on the PF_6^- salts of the nickel and palladium $M_2Cl_2(eHTP)^{2+}$ complexes. Once the non-hydrogen atomic coordinates had been input into the SYBYL program, hydrogen atoms were calculated into idealized positions and the terminal ethyl groups were converted into methyl groups to simplify the VDW calculation. We did perform a test calculation with the full eHTP ligand system and found that the terminal ethyl groups could almost always be rotated out of the way to give a conformation of energy similar to that observed with the methyl-substituted model system. Given the qualitative nature of these calculations the use of terminal methyl groups represents an excellent simplifying approximation.

The result of the VDW energy calculation on the PF_6^- salt of $Ni_2Cl_2(eHTP)^{2+}$ (**2c**) is very similar to that previously seen for the chloride salt (**2a**).[5] The previously reported VDW energy map for the chloride salt **2a** has, in some cases, considerably expanded energy contours[5] relative to that seen in the present calculation on **2c**. The reason for this is that the VDW energy evaluation scheme previously used in the SYBYL molecular mechanics program version 3.4 has been modified and updated in the current version 5.1. We consequently recalculated the VDW energy map for the chloride salt structure **2a** and found that the map had contracted contour values very similar to that seen here. Most importantly, the location of the global and local minima did not change.

The nickel and palladium calculations are summarized in Figures 4 and 5, which show contour plots of expanded portions of the full 360° × 360° energy maps. The contours signify increments in the VDW energies of 1.0, 5.0, and 20 kcal/mol, with the axes representing rotation angles about the two central methylene–phosphorus bonds. The origin of the plot (0°, 0°) corresponds to the inaccessible closed-mode configuration **1a**. In order for eHTP to form a closed-mode metal dimer, the P_{ex}–M–P_{ex} angle would have to be less than about 130°.

Discussion

Nickel Structures. We previously reported the synthesis and crystal structures of the Cl^- (**2a**) and BF_4 (**2b**) salts of $Ni_2Cl_2(eHTP)^{2+}$, which have distorted square-planar geometries about both nickel atoms and open-mode eHTP conformations.[5] van der Waals (VDW) energy calculations on the chloride salt structure of $Ni_2Cl_2(eHTP)^{2+}$ indicated the presence of several possible low-energy rotational conformations.[5] The lowest energy conformation agreed well with that seen for the crystal structure on the chloride salt **2a**, while the second lowest energy configuration was qualitatively quite similar to that seen for the structure on the BF_4^- salt, **2b**. In order to more fully probe the qualitative correctness of the van der Waals energy calculations on this system, we have now examined the X-ray structure on the PF_6^- salt of $Ni_2Cl_2(eHTP)^{2+}$, **2c**.

We will be using the syn and anti nomenclature to specify the general orientation of the metal centers in these rotationally flexible bimetallic complexes with respect to the hydrogen atoms on the central methylene bridge in eHTP: syn will refer to the presence of a metal center on the same side of the methylene group as the P–CH_2–P hydrogen atoms; anti will refer to the more conventional orientation in which a metal atom is located on the opposite side of the central methylene group. Thus, we will refer to conformer **1a** as anti,anti; **1b** as syn,syn, and **1c** as syn,anti.

The local coordination geometry about the nickel centers in **2c** is similar to that seen for **2a** and **2b**, as well as for the mononuclear complex[9] $[NiCl[PhP(CH_2CH_2PPh_2)_2]]^+$, except that the distortions away from square-planar geometry are more pronounced relative to the mononuclear system. The trans P–Ni–P angle in **2c** is the most distorted with a value of 156.28 (8)° for P2–Ni1–P3, which is essentially the same as that seen in the Cl^- (158.49 (4)°) and BF_4 (156.77 (6)°) salts. This rather severe distortion arises in part from the steric strain of having two fused five-membered chelate rings in a transoidal orientation (vide infra). The cisoidal P–Ni–P angles, for example, are compressed from 90° and range from 86.24 (7)° to 87.43 (7)° due to the five-membered chelate rings. The Ni–P bond distances are relatively short and range from 2.11 to 2.20 Å. The shortest M–P bond distances are for the central Ni–P1,4 bonds: Ni1–P1 = 2.114 (2) Å and Ni2–P4 = 2.122 (2) Å.

(8) (a) Naruto, S.; Motoc, I.; Marshall, G. R.; Daniels, S. B.; Sofia, M. J.; Katzenellenbogen, J. A. *J. Am. Chem. Soc.* **1985**, *107*, 5262. (b) The SYBYL program set is available from Tripos Associates, Inc., 1699 S. Hanley Rd., Suite 303, St. Louis, MO 63144.

(9) Bertinsson, G.-I. *Acta Crystallogr., Sect. C.: Cryst. Struct. Commun.* **1983**, *C39*, 563.

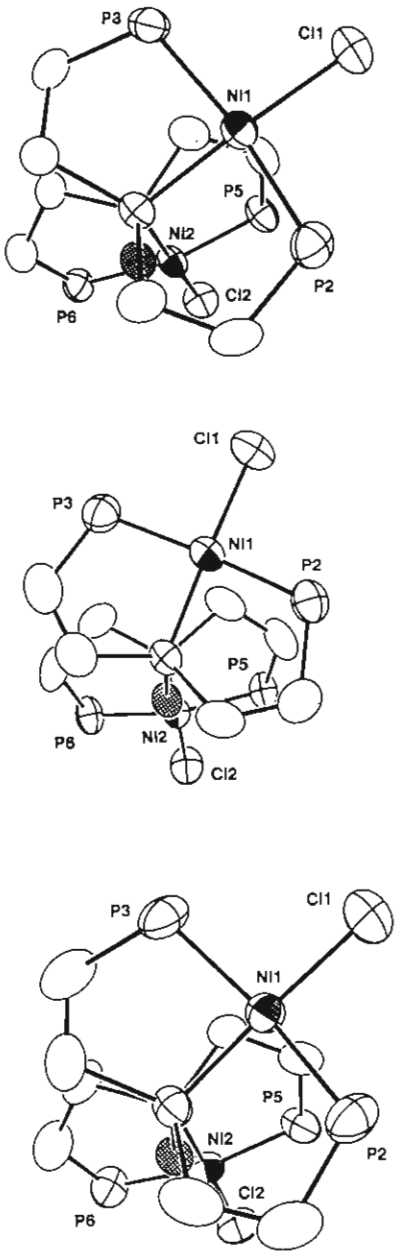

Figure 2. ORTEP plots looking down the P1···P4 vector for the three structurally characterized salts of $Ni_2Cl_2(eHTP)^{2+}$: Cl^- salt (**2a**); BF_4^- salt (**2b**); PF_6^- salt (**2c**). The central methylene group is oriented down in all three plots and has been hatched to highlight it as a reference point. The ethyl groups on the terminal phosphines have been omitted for clarity. Thermal ellipsoids are shown at the 33% probability level.

The overall ligand configuration for **2c** is about midway between the open-mode structures **1b** (syn–syn, W-shaped) and **1c** (syn–anti, scyth-shaped) and is most similar to the rotational conformation seen for the chloride salt **2a**. This is most clearly reflected in the Ni1–P1···P4–Ni2 torsional angles for the three salts: 93° (**2a**), 146° (**2b**), and 105° (**2c**). ORTEP plots of the three salts looking down the central P1–P4 vector clearly showing these rotational orientations are presented in Figure 2. The Ni–Ni separations are also related to the rotational conformation of the eHTP ligand with the distances roughly paralleling the Ni1–P1···P4–Ni2 torsional angles: 5.7505 (6) Å (**2a**), 5.9333 (8) Å (**2b**), and 5.885 (1) Å (**2c**). The other factor that affects the M–M separation is the angle about the central methylene group of the eHTP ligand. The P–CH_2–P angles seen in the Cl^-, BF_4^-, and PF_6^- structures are 120.9 (2)°, 122.5 (3)°, and 123.3 (3)°, respectively. These are all smaller than the value of 127.7 (3)° seen in the syn,syn complex $Co_2(CO)_4(eHTP)^{2+}$.

One interesting structural feature of $Ni_2Cl_2(eHTP)^{2+}$ is the considerable difference between the values observed for the trans

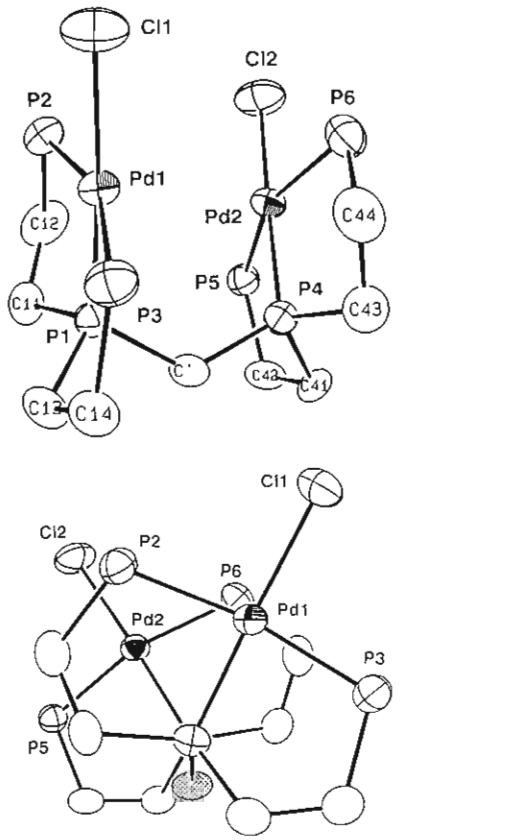

Figure 3. ORTEP plots of parallel and perpendicular views of $[Pd_2Cl_2(eHTP)](PF_6)_2$, **3**. The platinum structure is essentially isostructural to that shown here (see text for discussion). The ethyl groups on the terminal phosphines have been omitted for clarity in both views. Thermal ellipsoids are shown at the 33% probability level.

P–Ni–P angles about the two Ni atoms. The structure of **2c** reported here, for example, has a transoidal P2–Ni1–P3 angle of 156.28 (8)°, while the related Pd–Ni2–P6 angle about the other nickel atom is almost 11° larger, 167.11 (9)°. Similar trends are seen in the structures of **2a** and **2b**. The remaining L–M–L angles are, however, about the same for each half of the complex. These differences arise from the natural asymmetry of the syn,anti rotational conformation of the eHTP ligand. When the eHTP molecule is rotated into a syn,anti conformation, the anti trisphosphine half of the ligand experiences more steric crowding than the syn half. Furthermore, the worst steric contacts on the anti side occur for a square-planar orientation of the phosphine groups. This can be seen to a certain extent in Figure 1 where P2 and P3 (the *anti*-phosphines) are sterically interacting with the bridging ethylene linkages, C41 through C44, on the syn half of the ligand. P5 and P6, on the other hand, are well separated from the anti P1, P2, P3 half of eHTP. The increased steric crowding for P2 and P3, coupled with the weaker square-planar ligand field for nickel, is the root cause of the substantially larger distortion in the P2–Ni1–P3 angle.

Palladium and Platinum Structures. The structures on the palladium and platinum $M_2Cl_2(eHTP)^{2+}$ cations are essentially isostructural and, as with the nickel complexes, have somewhat distorted square-planar environments about the metal atoms. ORTEP plots of parallel and perpendicular views of the $Pd_2Cl_2(eHTP)^{2+}$ molecule are shown in Figure 3 (the Pt structure is nearly identical). Selected bond distances and angles are listed in Table V. The maximum deviations from square-planar geometry occur for the transoidal P–M–P angle, which has an average value of about 160° for the palladium system and 163° for the platinum complex. An expected difference between the Ni and Pd/Pt structures is that the metal to external phosphorus ($M–P_{ext}$) bond distances are longer for the Pd/Pt complexes with average values of 2.32 and 2.31 Å for Pd and Pt, respectively, compared to 2.20 Å for Ni. The metal to internal phosphorus

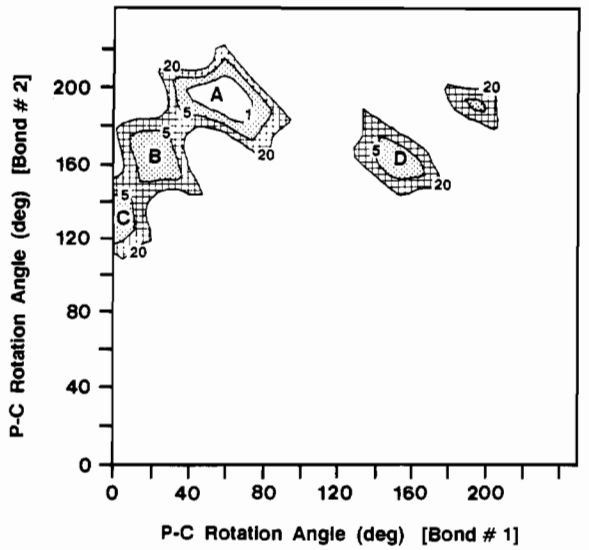

Figure 4. Expanded portion of the van der Waals (VDW) energy map for a model complex of $Ni_2Cl_2(HTP)^{2+}$ with methyl groups on the terminal phosphine groups. Axes indicate rotational angles about the two P–CH_2–P bonds with contours depicting relative VDW energies in kcal/mol with respect to the global minimum up to a maximum contour value of 20 kcal/mol. The location of the global minimum is labeled A which is only 5° away from the structurally observed conformer **2c**. Other local minima are labeled in terms of increasing energy and are labeled B, C, and D.

($M-P_{int}$) bond distances are also somewhat lengthened with values of 2.114 (2) and 2.122 (2) Å for Ni, 2.216 (2) and 2.206 (2) Å for Pd, and 2.197 (4) and 2.200 (4) Å for Pt. The shorter $M-P_{int}$ distances seen in the Ni and Pt species are consistent with the smaller size of the nickel atoms and the stronger Pt–P bonding relative to palladium.

The most obvious difference between the Ni and Pd/Pt structures, however, is in the rotational conformation of the M_2(eHTP) unit. The Pd and Pt structures have a partially closed mode, *anti,anti*-eHTP geometry. This can be clearly seen in the perpendicular view of the $Pd_2Cl_2(eHTP)^{2+}$ molecule in Figure 3. The M1–P1··P4–M2 torsional angles are 58° for Pd and 62° for Pt. The M–M separations also clearly reflect the partially closed mode configuration with Pd–Pd = 4.4217 (8) Å and Pt–Pt = 4.6707 (9) Å, which are quite a bit shorter than the values of 5.7–5.9 Å seen in the nickel systems. The anti,anti type eHTP orientation seen here is intrinsically more symmetrical than the syn,anti conformations seen for the bimetallic nickel systems. There is an approximate 2-fold rotation axis that passes through the central methylene group of the eHTP ligand for the Pd and Pt complexes as can be seen in Figure 3. This more symmetrical structure implies that the steric interactions on both sides of M_2(eHTP) should be similar and this is indeed reflected by the fact that the local coordination environments about both palladium and platinum metal atoms are essentially the same, in sharp contrast to the significant asymmetry observed in the syn–anti nickel complexes.

A remarkable feature of the platinum structure is the 129.7 (9)° angle observed for the central eHTP P–CH_2–P bridge. Until recently this value was the largest methylene bridge angle observed, similar to the 129.3° methylene bridge angle found in bis(9-triptycyl)methane by Mislow and co-workers.[10] Singleton and co-workers, however, have reported the first example of a bimetallic transition-metal system with a bis(diphenylphosphino)-methane (dppm) ligand that has the inverted syn,syn P–CH_2–P orientation that was originally observed in $Co_2(CO)_4(eHTP)^{2+}$,[2] namely, $[\{(\eta^5\text{-}C_5H_5)Ru(1,10\text{-phen})\}_2(\mu\text{-dppm})]^{2+}$, which has the extraordinarily large methylene bridge angle of 133.1 (3)°.[11] The palladium structure has a smaller P–CH_2–P angle of 126.6 (4)°, which is almost exactly midway between the values of 123.3 (3)° and 129.7 (9)° seen for the nickel and platinum systems. It is tempting to correlate the increasing angular values simply to the increasing size of the metal atoms and while the radius of the metal center certainly does have some effect, we will see that the root cause is more complex.

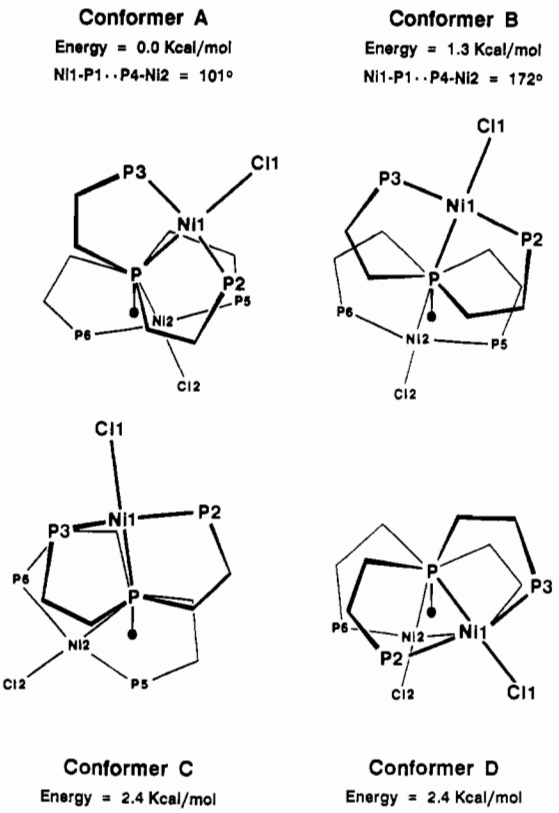

Figure 5. Calculated low-energy rotational conformations from the SYBYL VDW energy calculations for the model complex of $Ni_2Cl_2(HTP)^{2+}$. The views are all looking directly down the central P1··P4 axis. The methyl groups on the terminal phosphorus atoms have been omitted for clarity and the central methylene group is oriented down in each view and emphasized with a heavy dot. The labeling scheme used is the same as that in the ORTEP plots (Figures 1 and 2). Calculated VDW energies and Ni1–P1··P4–Ni2 torsional angles are listed for each conformer.

Nickel van der Waals Energy Calculation. The nickel calculation, shown in Figure 4, clearly shows that there are four low-energy regions with the crystallographically observed rotomer, **2c**, lying only 5° from the global minimum, which has been marked with the label A. The next lowest energy rotomer falls in the center of region B and has a VDW energy of only +1.3 kcal/mol above the global minimum. The conformers that reside in the regions labeled C and D both have equivalent VDW energies of +2.4 kcal/mol. Stick diagram representations of these four rotational configurations looking down the central P1··P4 vector are shown in Figure 5 where both hydrogen atoms and methyl groups on the terminal phosphines have been omitted for clarity. In each view the central methylene group is pointed down and emphasized by a heavy dot. Rotomers A, B, and C are all syn–anti types and have Ni1–P1··P4–Ni2 torsional angles of 101°, 172°, and 113°, respectively. Conformer D, on the other hand, is a syn–syn system analogous to **1b** and the basic structure seen for $Co_2(CO)_4(eHTP)^{2+}$.[2]

In addition to identifying favored low-energy configurations for our nickel eHTP complex, the calculation also gives valuable information about the availability of energetically reasonable pathways from one rotomer to another. Since the torsional energies involved for rotations about single bonds are minimal, the VDW energies should be the primary contributing factors to any rotational barrier considering the constraints of our simple static system. The calculations indicate that there are very low barriers for rotations from regions A ⇌ B ⇌ C. The barrier from region

(10) Johnson, C. A.; Guenzi, M.; Nachbar, R. B., Jr.; Blount, J. F.; Wennerstrom, O.; Mislow, K. *J. Am. Chem. Soc.* **1982**, *104*, 5163.
(11) Albers, M. O.; Liles, D. C.; Robinson, D. J.; Singleton, E. *Organometallics* **1987**, *6*, 2179.

C to B is only 7 kcal/mol, while the barrier from B to A is 8 kcal/mol. The barrier from A to C, however, is a relatively high 51 kcal/mol.

It is important to point out that the energies from the VDW energy calculation should be formally treated as approximate and qualitative in nature. Except for the two rotatable P–CH_2–P bonds, our model assumes a static molecule based on the geometric parameters obtained from the crystal structure. It has been demonstrated that energies from the SEARCH routines in SYBYL for geometry optimizations in cyclic systems do not generally constitute a reliable criteria for choosing potential structures since they tend to *overestimate* atom–atom interactions in these nonoptimized systems.[12] The net result is that while all the calculated energies are overestimated, the higher energy values from the calculation are the most overestimated. As we will see, this limitation on the accuracy of the VDW energies will not hinder our qualitative interpretations of the results.

For example, the group VI eHTP-based bimetallic carbonyl systems $M_2(CO)_6$(eHTP) (M = Cr, Mo, W) have been structurally characterized and form an isomorphous series of structures that have an open-mode anti,anti geometry in which the two halves of the complex are symmetrically splayed apart by ca. 102° giving M–M separations of 6.3–6.5 Å.[3] Spectroscopic studies and VDW energy calculations provide strong evidence, however, that in CH_2Cl_2 solution the anti–anti $M_2(CO)_6$(eHTP) solid-state structure rotates about the central eHTP methylene group to give a syn–anti solution orientation similar to **1c**. Thus, these "simplistic" VDW calculations have proven to be extremely useful in our conformational studies.

Because of the rigid model being used and the simplicity of the VDW calculation, we estimate that for the low-energy regions values within ca. 2 kcal/mol should be considered approximately equivalent. In spite of this, we will continue to report energy values typically to one decimal place. The 51 kcal/mol barrier between A and D is an example of the overestimation of VDW energies and the danger of reading too much into one specific number. Increasing the central methylene bridge angle by only 2.7° to 126.0°, for example, causes a major drop in the A ⇄ C barrier to 18 kcal/mol. It is very likely that other minor twisting and deformation motions of the Ni_2(eHTP) unit could also assist in the lowering of this barrier energy. We therefore believe that all four conformers are energetically accessible, with conversions between A ⇄ B ⇄ C being particularly facile.

Palladium VDW Energy Calculation. The VDW rotational energy map for $Pd_2Cl_2(HTP)^{2+}$ is shown in Figure 6. Due to the similarity between the Pd and Pt structures and their VDW energy maps, we will concentrate the discussion on the palladium complex. The axes and relative VDW energy contour values (1, 5, and 20 kcal/mol) for the Pd map are the same as that used in the Ni calculation. The energy map, however, is substantially different in two ways; there is a relatively large region of low-energy anti–anti conformers near the origin and an approximate mirror plane of symmetry across the diagonal of the map. The increased symmetry of the VDW energy map comes from the more symmetrical structure of $Pd_2Cl_2(HTP)^{2+}$, which has an approximate 2-fold rotation axis passing through the central methylene bridge and can be contrasted to the far less symmetrical syn–anti $Ni_2Cl_2(HTP)^{2+}$ structure (vide supra). The asymmetries in the map primarily arise from the fact that the two chelate rings about each metal center have somewhat different conformations. In solution we expect these differences to average out to give a completely symmetrical system.

The global minimum for the palladium complex is labeled A and is essentially the same rotational conformation seen for the nickel system. There is, however, a second conformer that is only 0.04 kcal/mol higher in energy at the position labeled B. Considering the accuracy of these simple VDW energy calculations, conformations A and B should certainly be considered isoenergetic. The observed crystal structure for $Pd_2Cl_2(HTP)^{2+}$ is only 5° away from B with a VDW energy of 0.6 kcal/mol. Once again these VDW energy calculations are in almost quantitative agreement with the observed crystal structures. The conformation labeled C is similar to rotamer B from the nickel calculation and has an energy of 1.8 kcal/mol. The syn–syn conformer located at position D (2.0 kcal/mol) is, again, almost exactly analogous to that seen for nickel. As with the nickel system, the energy barriers for rotations between A ⇄ C ⇄ B are low: A ⇄ C = 14 kcal/mol; C ⇄ B = 6 kcal/mol. The barrier between A and D is considerable with an average value of 136 kcal/mol. We believe that this barrier height is overestimated although it is most probably higher than in the nickel system for reasons discussed below.

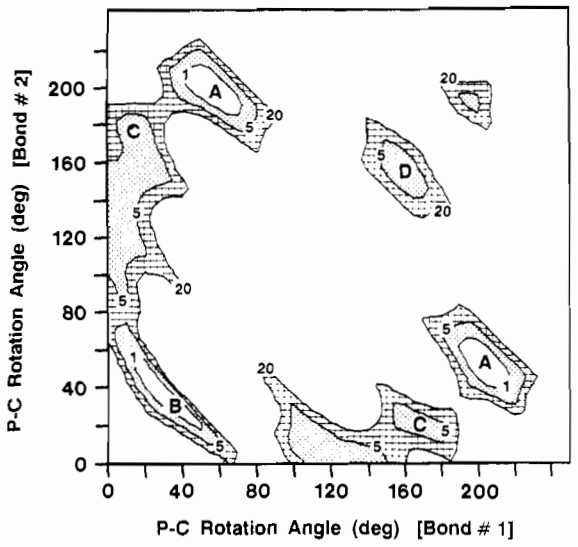

Figure 6. Expanded portion of the VDW energy map for a model complex of $Pd_2Cl_2(HTP)^{2+}$. The axes and energy scale are identical with that used in Figure 4 for the nickel system. The location of the global minimum is labeled A, while the other local minima are labeled in terms of increasing energy are labeled B, C, and D. Conformer B is located at the position of the crystallographically determined structure.

What the VDW map does not directly tell us is why the nickel complex does not appear able to access the anti–anti conformation B seen in the crystal structure of $Pd_2Cl_2(HTP)^{2+}$. One obvious factor is the angle of the central P–CH_2–P linkage. On the basis of VDW energy calculations, however, simply opening up the nickel methylene bridge angle of 123.3° to the 126.6° value seen for palladium does *not* allow the nickel system to access the anti–anti rotational conformation. The reason for this can be studied by using the SYBYL program to do a least-squares superpositioning of the Pd structure with a model $Ni_2Cl_2(HTP)^{2+}$ structure that has a 126.6° P–CH_2–P bridge angle and has been rotated into the same rotational conformation as the Pd structure. When the Ni and Pd systems are so overlapped, it becomes immediately obvious that the Ni2 half of the complex is substantially bent toward the Ni1 side (a stereopair diagram of these two superimposed molecules is included in supplementary material). Although the Ni2··Pd2 difference for the two overlapped molecules is only 0.44 Å, the C61(Ni)··C61(Pd) difference is a very large 1.79 Å. This brings the nickel C61 methyl grup to within 1.88 Å of Cl1. It is this very unfavorable intramolecular interaction of the C61 methyl group with Cl1 in the nickel VDW calculation that disfavors the rotational conformation seen in the Pd/Pt systems.

There are two structural factors, aside from the central methylene bridge angle, that have considerable impact on the C61··Cl1 contact: the C′–P4–Ni2 and P5–Ni2–P6 angles. The C′–P4–Ni2 angle in **2c**, for example, is 109.4 (2)° while values of 120.8 (3)° and 122.7 (6)° are seen in the Pd and Pt structures. Similarly the more linear P5–Ni2–P6 angle (167.11 (9)°) in the nickel system works to "bend" the C61 methyl group toward the Ni1 half of the complex relative to the more highly distorted P5–M–P6 angles seen for Pd and Pt: 159.24 (8)° (Pd) and 163.5 (2)° (Pt). The reason for these differences arises, once again, from the asymmetric nature of the syn–anti $Ni_2Cl_2(HTP)^{2+}$

(12) Richards, A. (Tripos Associates), Tripos Users Meeting, St. Louis, MO, June 1987.

structure. Remember that the syn-N_2 half of this bimetallic complex exists in the least sterically demanding site and the bond angles reflect this by lying closer to their ideal square-planar values. Since we are using the crystal structures as a starting point for our VDW energy calculations, it is natural that any structural biases present are also carried through into the calculations. By modifying the C′–P4–Ni2 and P5–Ni2–P6 angles to that seen for Pd, we get a much improved superposition of the two molecules and a VDW energy map for Ni that is qualitatively the same as the Pd map.

Since it is no doubt energetically reasonable for the nickel system to adopt the angles seen in the Pd system, it is equally likely that it could also adopt the anti,anti conformer seen for the palladium and platinum structures. One reason the nickel complex does not seem to want to crystallize in the anti,anti conformer is because the weaker square-planar ligand field about the nickel atom allows the ligands to distort enough to favor, on an *overall* energy basis, the observed syn,anti conformations. The VDW energy calculations only give information about intraligand steric factors and a nonchanging set of C–H, C–C, and C–P bond stretching, bending, torsional energies. We have to qualitatively mix in our chemical knowledge about the geometric preferences of the metal centers to arrive at an overall picture for this transition metal based system.

The increased P–CH_2–P bridge angle in the Pt complex is caused in large part by the stronger square-planar ligand field for platinum relative to palladium. The P_{ext}–M–P_{ext} angles for the Pd complex (160.11 (8)° and 159.24 (8)°) show a somewhat greater spread and are distorted further away from square-planar than those for Pt (163.6 (2)° and 163.5 (2)°). Because of the length of the M–P–Et moment arm (Me groups in the calculated model system) and the fact that the ethyl groups on the external phosphines are the major contributors to the intramolecular steric contacts, even a small change in the P_{ext}–M–P_{ext} angle will have an enhanced effect on the P_{int}–C′–P_{int} and C′–P_{int}–M angles. In this case the movement of the P_{ext}–M–P_{ext} angle toward planar moves the endo ethyl groups toward the other half of the M_2-(eHTP) complex increasing the intramolecular steric contacts. The Pt system compensates by increasing both the P_{int}–C′–P_{int} and average C′–P_{int}–M angles to 129.7 (9)° and 121.5°, respectively, relative to values of 126.6 (4)° and 120.9° for Pd.

NMR Studies on $Ni_2Cl_2(eHTP)^{2+}$. The ^1H NMR spectra of $Ni_2Cl_2(eHTP)^{2+}$ (**2**) show solvent and, in some cases, anion dependence as illustrated in Figure 7. Perhaps the most obvious shift occurs for the central methylene group (P–CH_2–P) triplet resonance where it shifts downfield by 0.6 ppm in acetone-d_6 relative to MeCN-d_3 or CD_2Cl_2. There are also numerous other smaller shifts in the positions and splittings for the chelate ring protons. We have completely assigned the spectrum in the case of the PF_6^- salt in acetone-d_6 using two-dimensional ^1H *J*-correlated spectroscopy[13] and these assignments are listed in the Experimental Section.

The ^1H NMR spectral shifts result mainly from rotational motion about the central methylene bridge of the eHTP ligand allowing access to, and interconversions between, the various conformers of **2**. We have seen similar effects in the ^1H NMR spectra of $Co_2(CO)_4(eHTP)^{2+}$ where both rotational and geometric (trigonal bipyramidal ⇌ square pyramidal) conformations are seen.[14] Just as in the $Co_2(CO)_4(eHTP)^{2+}$ system, solvent effects could readily differentiate (or set up equilibria between) the various rotational conformers seen from the VDW energy calculations. Some of these conformers are expected to have different enough local chemical environments for the central methylene and bridging ethylene protons.

An interesting feature in the MeCN-d_3 spectrum of the chloride salt **2a** (^1H NMR spectra included in supplementary material) is the very low intensity triplet resonance at 3.9 ppm, which corresponds to the central methylene bridge protons. Since there is another triplet resonance of normal intensity at 2.45 ppm in the same spectrum, it would appear that in this solvent system one has two different static or slowly exchanging conformers present. The 1.4 ppm difference between these two resonances is very large, greater than the maximum shift of ca. 1.0 ppm observed for the various P–CH_2–P resonances in $Co_2(CO)_4$-(eHTP)$^{2+}$.[14]

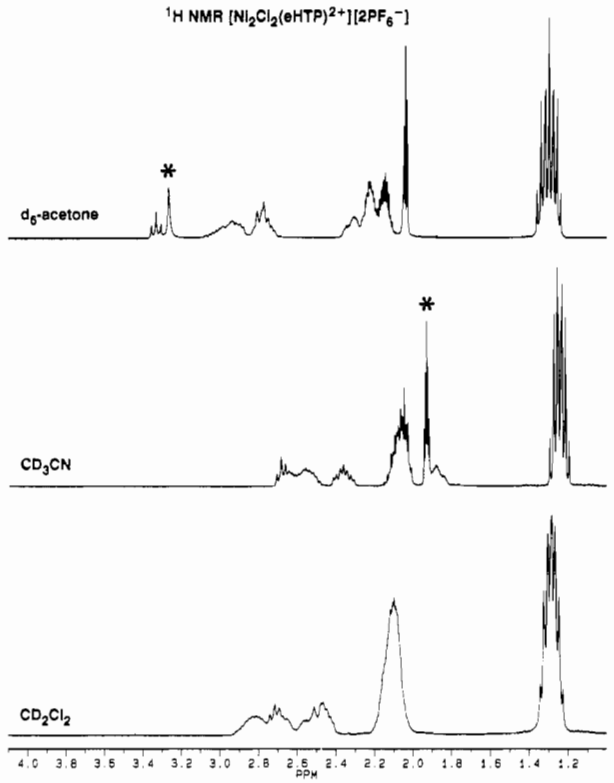

Figure 7. 400-MHz ^1H NMR spectra of $[Ni_2Cl_2(eHTP)](PF_6)_2$ in the solvents indicated. Starred peaks are due to solvent.

This large chemical shift difference is puzzling. The shifting of the P–CH_2–P resonances in the case of $Co_2(CO)_4(eHTP)^{2+}$ was explained by the presence of different rotational conformers which give rise to varying amounts of nuclear shielding from the carbonyl groups which are in close proximity to the hydrogen atoms of the central methylene bridge. Yet we do not have the potential shielding effect of carbonyl groups in **2**. In the previous report[5] on the nickel complexes we proposed that in the presence of chloride anions one could have chloride association and dissociation reactions occurring which would give rise to an equilibrium between the neutral five-coordinate $Ni_2Cl_4(eHTP)$ complex and **2** and this could be one explanation for the large shift in the methylene bridge resonance.

This has been studied by taking a d_3-MeCN solution of chloride ion in the form of Ph_4AsCl and gradually adding it to a PF_6^- salt solution of **2** while monitoring the ^1H NMR and UV–vis spectra. Only small changes in the ^1H NMR spectrum were observed and no changes in the UV–vis spectrum were seen. Four- and five-coordinate Ni(II) complexes have relatively different electronic absorption spectra,[15] and if a five-coordinate $NiCl_2(P_3)$ species was forming, one would expect to see some change in the UV–vis spectrum. We attribute the minor changes in the ^1H NMR spectrum to rotational differences in **2** caused by the difference in the ionic strength and dielectric constant of the salt/solvent system. One potential problem with this study is that the Ph_4AsCl may be present as a tightly associated ion pair in acetonitrile and is not providing a ready source of chloride ions.

Conclusions. The homobimetallic eHTP complexes of Ni^{2+}, Pd^{2+}, and Pt^{2+} are all similar in that they do not have any M–M interactions and have the eHTP ligand bonding in a "*traditional*"

(13) Aue, W. P.; Karhan, J.; Ernst, R. R. *J. Chem. Phys.* **1976**, *65*, 4226.
(14) D'Avignon, A.; Askham, F. R.; Stanley, G. G. *Inorg. Chem.* **1990**, *29*, 3363.
(15) Cf. Lever, A. B. P. *Inorganic Electronic Spectroscopy*, 2nd ed.; Elsevier: Amsterdam, 1984.

tridentate fashion to each metal center. These complexes, however, posses considerable rotational flexibility about the central eHTP methylene bridge giving rise to a number of low energy rotational conformations. The various conformations of these systems have been probed by X-ray crystallography, NMR spectroscopy, and VDW energy calculations. Although the VDW energy calculations are quite crude, they provide an excellent qualitative road map to the conformations accessible to these systems and provide considerable insight into understanding the structural differences between the Ni and Pd/Pt complexes.

The rotational flexibility of these systems could be extremely important in allowing the metals to access one another for cooperative bimetallic behavior. One reaction that is potentially well suited to binuclear systems is hydroformylation and there have been several reports on the effects of homo- and heterobimetallic homogeneous catalysts on the rate and selectivity of hydroformylation reactions.[16,17] We are, therefore, particularly interested in studying the hydroformylation activity of bimetallic complexes based on our considerably less sterically hindered binucleating *tetra*phosphine ligand system $(Et_2PCH_2CH_2)(Ph)PCH_2P(Ph)(CH_2CH_2PEt_2)$, eLTTP.[18-20] This ligand has essentially the same bridging/chelating coordinating properties as eHTP, yet will readily allow two square-planar metal centers to come into close proximity. Indeed, it is in large part these conformational studies on eHTP complexes of the group 10 metals that lead to the design and synthesis of the eLTTP ligand system.

Acknowledgment. We thank the National Science Foundation (Grants CHE-86-13089 and CHE-88-23041) for research support and Dr. Frank R. Fronczek (LSU) for collecting the X-ray data on the palladium system. We also acknowledge the helpful comments of the manuscript reviewers.

Supplementary Material Available: A stereopair figure of the SYBYL least-squares overlapped structures of $Ni_2Cl_2(HTP)^{2+}$ and $Pd_2Cl_2(HTP)^{2+}$, the ^1H NMR spectra of **2a** in CD_3OH, CD_3CN, and CD_2Cl_2, and Tables S-I-S-IV of crystal and data collection parameters and anisotropic thermal parameters (10 pages); Tables S-V and S-VI of observed and calculated structure factors (33 pages). Ordering information is given on any current masthead page.

(16) Sanger, A. R. *Homogeneous Catalysis with Metal Phosphine Complexes*; Pignolet, L. H., Ed.; Plenum: New York, 1983; pp 215-237.
(17) (a) Gelmini, L.; Stephan, D. W. *Organometallics* **1988**, *7*, 849. (b) Kovacs, I.; Hoff, C. D.; Ungvary, F.; Marko, L. *Organometallics* **1985**, *4*, 1347. (c) Hidai, M.; Fukoka, A.; Koyasu, Y.; Uchida, Y. *J. Chem. Soc., Chem. Commun.* **1984**, 516. (d) Pino, P.; von Bezard, D. A. Swiss Patent 625,233, 1981.
(18) Laneman, S. A.; Fronczek, F. R.; Stanley, G. G. *J. Am. Chem. Soc.* **1988**, *110*, 5585.
(19) Laneman, S. A.; Fronczek, F. R.; Stanley, G. G. *Inorg. Chem.* **1989**, *28*, 1206.
(20) Laneman, S. A.; Fronczek, F. R.; Stanley, G. G. *Inorg. Chem.* **1989**, *28*, 1872.

Contribution from the Departamento de Química Inorgánica, Instituto de Ciencia de Materiales, Facultad de Química, Universidad de Sevilla-CSIC, Apartado 553, 41071 Sevilla, Spain, Instituto de Ciencia de Materiales, Sede D, CSIC, Serrano 113, 28006 Madrid, Spain, and Facultad de Ciencias Químicas, Universidad Complutense de Madrid, 28040 Madrid, Spain

Reactions of Sulfur-Containing Heterocumulenes with Low-Valent Molybdenum and Tungsten Complexes. Oxidative Cleavage of a Head-to-Tail Carbon Disulfide Dimer in a Molybdenum Complex

Ernesto Carmona,*[1a] Agustín Galindo,[1a] Angeles Monge,*[1b] Miguel Angel Muñoz,[1a] Manuel L. Poveda,[1a] and Caridad Ruiz[1b]

Received March 30, 1990

Head-to-tail carbon disulfide dimers of composition $M(C_2S_4)(C_2H_4)(PMe_3)_3$ (M = Mo (**3**), W (**4**)) have been prepared by action of CS_2 on the ethylene complexes *trans*-$M(C_2H_4)_2(PMe_3)_4$ (M = Mo (**1**), W (**2**)). An X-ray analysis, carried out on complex **3**, shows the C_2S_4 unit is acting formally as a four-electron donor ligand, η^3-bonded to the metal through one of the carbon and two of the sulfur atoms. The complex is monoclinic, $C2/c$, with a = 26.633 (7) Å, b = 8.615 (4) Å, c = 19.903 (6) Å, β = 103.51 (2)°, and D(calcd) = 1.60 g cm^{-3} for Z = 8 and $R(F_o)$ = 0.048. The analogous reactions of **1** and **2** with SCNPh provide related head-to-tail dimers, $Mo(S_2C_2(NPh)_2)(C_2H_4)_x(PMe_3)_{4-x}$, ($x$ = 1 (**7**); x = 2 (**8**)) and $W(S_2C_2(NPh)_2)(C_2H_4)_x(PMe_3)_{4-x}$, ($x$ = 1 (**9**); x = 2 (**10**)). Treatment of **3** with MeX (X = I, OSO_2CF_3), followed by anion exchange with NH_4PF_6, gives $[Mo(C_2S_4Me)(C_2H_4)(PMe_3)_3]PF_6$ (**11**), which has a structure similar to that found for **3** (as determined by X-ray studies) but with a methyl group bonded to the exocyclic sulfur atom of the C_2S_4 unit. **11** is monoclinic, $P2_1/c$, with a = 13.726 (2) Å, b = 14.272 (3) Å, c = 14.686 (4) Å, β = 106.28 (2)°, and D(calcd) = 1.509 g cm^{-3} for Z = 4 and $R(F_o)$ = 0.058. Complex **3** reacts with $CNBu^t$ to afford a complex mixture of compounds from which the substitution product $Mo(C_2S_4)(CNBu^t)(PMe_3)_3$ (**12**) can be isolated. With carbon monoxide, however, a molybdenum(0) complex, $Mo(S_2CPMe_3)(CO)_2(PMe_3)_2$ (**13**), is formed in an unprecedented reaction that corresponds to an oxidative symmetric cleavage of the MC_2S_4 linkage.

Introduction

The interaction of heterocumulene molecules with transition-metal compounds has been extensively studied in the past decade, and a wealth of information is now available on their coordination modes and their metal-induced transformations.[2,3] Sulfur-containing heterocumulenes such as carbon disulfide, carbonyl sulfide, and organic isothiocyanates have received considerable attention and have been shown to form complexes with a number of transition metals and to undergo a variety of chemical transformations including insertion, dimerization, and disproportionation reactions.[3]

Electron-rich transition-metal compounds are able to promote the so-called reductive dimerization of carbon disulfide,[4] either

(1) (a) Universidad de Sevilla-CSIC. (b) CSIC and Universidad Complutense de Madrid.
(2) For recent reviews on CO_2 chemistry, see: (a) Behr, A. *Angew. Chem., Int. Ed. Engl.* **1988**, *27*, 661. (b) Braunstein, P.; Matt, D.; Nobel, D. *Chem. Rev.* **1988**, *88*, 747. (c) Walther, D. *Coord. Chem. Rev.* **1987**, *79*, 135.
(3) For recent reviews on CS_2 chemistry, see: (a) Bianchini, C.; Mealli, C.; Meli, A.; Sabat, M. In *Stereochemistry of Organometallic and Inorganic Compounds*; Bernal, I., Ed.; Elsevier: Amsterdam, 1986; Vol. 1, p 146. (b) Ibers, J. A. *Chem. Soc. Rev.* **1982**, *11*, 57. (c) Werner, H. *Coord. Chem. Rev.* **1982**, *43*, 165.

0020-1669/90/1329-5074$02.50/0